Bannier, E.; Vicent, M.; Rayón Encinas, E.; Benavente Martínez, R.; Salvador Moya, MD.; Sánchez, E. (2014). Effect of TiO2 addition on the microstructure and nanomechanical properties of Al2O3 Suspension Plasma Sprayed coatings. Applied Surface Science. 316:141-146. doi:10.1016/j.apsusc.2014.07.168.

Effect of TiO_2 addition on the microstructure and nanomechanical properties of Al_2O_3 Suspension Plasma Sprayed coatings

E. Bannier[1], M. Vicent[1], E. Rayón*[2], R. Benavente[2], M. D. Salvador[2], E. Sánchez[1]

[1] *Instituto de Tecnología Cerámica - Asociación de Investigación de las Industrias Cerámicas. Universitat Jaume I. Av. Vicent Sos Baynat s/n, 12006 Castellón, Spain*

[2] *Instituto de Tecnología de Materiales. Universitat Politècnica de Valencia. Camí de Vera s/n, E46022 Valencia, Spain.*

* *Corresponding author:*
Name: Emilio Rayón Encinas
phone: (+34) 660806113
fax : (+34) (+34) 963877629
e-mail: emraen@upvnet.upv.es

ABSTRACT

Alumina-titania coatings are widely used in industry for wear, abrasion or corrosion protection components. Such layers are commonly deposited by atmospheric plasma spraying (APS) using powder as feedstock. In this study, both Al_2O_3 and Al_2O_3-13 wt% TiO_2 coatings were deposited on austenitic stainless steel coupons by suspension plasma spraying (SPS). Two commercial suspensions of nanosized Al_2O_3 and TiO_2 particles were used as starting materials. The coatings microstructure and phase composition were fully characterised using FEG-SEM and XRD techniques. Nanoindentation technique was used to determine the coatings hardness and elastic modulus properties. Results have shown that the addition of titania to alumina SPS coatings causes different crystalline phases and a higher powder melting rate is reached. The higher melted material achieved, when titania is added leads to higher hardness and elastic modulus when the same spraying parameters are used.

Keywords: Suspension plasma spraying; Nanostructured coatings; Alumina; Titania; Nanoindentation

1. Introduction

Nanostructured materials have been extensively studied in the past decades [1-3] showing that nanostructure significantly increases material performances [4-6]. In particular, nanostuctured coatings are expected to provide several industries with enhanced components leading to better properties and longer lifetime [7-9]. Atmospheric Plasma Spraying (APS) is one of the most widely used techniques in industry to deposit thick ceramic coatings. APS process consists in injecting a powder into a plasma plume. During the flight in the plasma, the feedstock is molten and accelerated towards a substrate where it impacts creating a coating [10].

The production of nanostructured coatings by APS, requires to agglomerate the nanoparticles into micrometer sized aggregates, which can be sprayed as easily as conventional powders [11-13]. The use of agglomerated powders is actually considered as a very efficient way to deposit a coating based on nanoparticles. However, the production of aggregated powders is a complex process with several steps [13-14] which affect the cost of powders and may restrict the possible industrial applications. Moreover, a big challenge is to carefully control the deposition process in order to keep the initial nanostructure in the final coating [15]. Some example of nanostructured ceramic coatings obtained by APS from agglomerated powders include alumina [16,17], titania [18,19], alumina-titania [14,20], yttria-stabilised zirconia [21,22] or pyrochlore [23].

Another possible way to obtain nanostructured coating by thermal spraying consists of using a carrier liquid instead of a carrier gas to inject the nanoparticles inside the plasma

plume [12]. This technique is known as Suspension Plasma Spraying (SPS) and differs significantly from conventional APS since the suspension is fragmented into droplets and the liquid phase vaporised before the solid feedstock is processed [24,25]. This novel technique has recently undergone an extensive development, leading to the deposition of nanostructured coatings with unique properties for solid oxide fuel cells (SOFC) functional layers [28,29], thermal barrier coatings [30,31], photocatalytic layers [32,33], wear resistant coatings [34] or bioactive layers [35].

Among the materials usually deposited by plasma spraying, alumina-based coatings show one of the most versatile field of application [36]. Alumina is commonly used as an electrical insulator due to its high dielectric strength and its ability to manufacture hard and chemically stable coatings even at very high temperatures. Furthermore, Al_2O_3-based coatings are widely used for wear, corrosion or erosion protection components. In such coating alumina is mixed with other oxides to enhance its properties. It has been shown that the addition of TiO_2 improves the coating fracture toughness in conventional APS coatings [36]. Indeed Al_2O_3-TiO_2 coatings obtained by APS from both conventional feedstocks and agglomerated powders has been extensively studied [37-44]. However, the research on SPS Al_2O_3-TiO_2 is still incipient and very few authors have studied such layers [45]. Consequently, it is still necessary to study the effect of the addition of TiO_2 on the characteristics of alumina SPS coatings.

In the present work, both Al_2O_3 and Al_2O_3-13wt% TiO_2 coatings have been deposited by Suspension Plasma Spraying using two commercial aqueous nano-suspensions as feedstock. Resulting microstructures were fully characterised by FEG-SEM observations and X-Ray diffraction analysis. Furthermore, the mechanical properties (hardness and elastic modulus) of the coatings were characterised using the nanoindentation technique.

2. Material and methods

2.1. Materials

Coatings were deposited from an Al_2O_3-13wt% TiO_2 suspension prepared by mixing two commercial aqueous suspensions: a nano-Al_2O_3 suspension (AERODISP® VP630X, Evonik Degussa GmbH, Germany) and a nano-TiO_2 supension (AERODISP® W740X, Evonik Degussa GmbH, Germany), following the methodology described elsewhere [26]. The main nanosuspensions properties are summarised in table 1 as given by the manufacturer. Both suspensions have been fully characterised in previous works [26-27].

Stainless steel (AISI 304) disks have been used as substrates (25 mm diameter and 10 mm thickness). Before deposition, the substrates were grit blasted with corundum (Metcolite VF, Sulzer Metco, Switzerland) and cleaned with ethanol.

2.2. Coating deposition

Coatings were deposited with a F4-MB monocathode torch (Sulzer Metco, Switzerland) with a 6 mm internal diameter anode operated by a robot (IRB 1400, ABB, Switzerland). The substrates were preheated between 350 ºC and 400 ºC to enhance coating adhesion.

The suspensions were injected using a SPS system developed by the Institute for Ceramic Technology (Instituto de Tecnología Cerámica, ITC). This system is formed by two pressurised containers which force the liquid to flow through the injector. A filter was used to remove agglomerates larger than 74 μm and possible contaminations. Main spraying parameters are given in table 2.

2.3. Coating characterisation techniques

X-ray diffraction patterns were collected to identify crystalline phases in coating samples (Bruker, Theta-Theta D8 Advance, Germany).

The microstructure was analysed on polished cross-sections using a HITACHI S4800 Field Emission Microscope (FEG-SEM) under secondary (SE) and backscattered (BSE) electron mode. The BSE detector was configured symmetrically to ensure a good reflection of the backscattered electrons from all angles. Elemental analysis was performed in SEM using energy dispersive X-rays analysis (EDX). An optical reflection microscope Nikon LV-100 Eclipse under Nomarski illumination on the cross-section was used.

Hardness (H) and elastic modulus (E) of coatings were acquired by a G-200 nanoindenter from Agilent Technology (Santa Clara, USA). Indentations were performed at 2000 nm constant depth using the Continuous Stiffness Measurement (CSM) method that provides the stiffness profile in-depth and hence, the subsequent calculation of H and E. A Berkovich-geometry tip was used. The area function for this indenter was previously calibrated on silica as reference material.

3. Results

3.1. Crystalline phase composition

As reported elsewhere, commercial titania feed suspension is mainly formed by anatase with some rutile. In the case of the alumina starting suspension, it contains Alu-C nanoaparticles (Degussa/Evonik, Germany) [14] which are formed by transition δ- and γ-Al_2O_3 [46]. Figure 1 shows the X-ray diffraction patterns of both Al_2O_3 and Al_2O_3-TiO_2 projected coatings.

Figure 1

Pure alumina SPS coating was mostly formed by corundum (α-Al_2O_3) with δ-Al_2O_3. Traces of γ-alumina were also identified. This result indicates that powders have experimented a phase transformation during the deposition process which is usual in plasma spraying in both conventional and nanostructured alumina coatings [47,48]. The formation of α-Al_2O_3, which is the stable phase of the aluminium oxide, is of special interest due to its thermal stability and good mechanical properties.

When titanium oxide is added to the feed suspension, X-ray diffraction analysis revealed that the alumina found in the coating is mainly present as α-Al_2O_3 and γ–alumina phases. Low amounts of brookite-TiO_2 were also identified with traces of rutile. However most of the initial titania reacted with alumina during the deposition process, leading to the formation of aluminium titanate (Al_2TiO_5). This phenomenon has been previously reported for APS alumina-titania coatings with different TiO_2 content [38,40].

3.2. Microstructure

The microstructures of Al_2O_3+13wt%TiO_2 and Al_2O_3 coatings are shown in figure 2a and 2b, respectively. In both cases, a bimodal microstructure formed by a mixture of fully melted grains and softer lakes of material was observed. Nevertheless, when TiO_2 was added to the feedstock, a higher ratio of melted material was observed. The softer microstructure was probably formed by partially melted material. However it was not possible to observe the original nanostructure at higher magnifications, indicating that certain sintering degree was achieved.

Figure 2.

Venkataraman et al.[49] analysed Al_2O_3 with 13 wt.% TiO_2 coatings by BSE and they found that the α-alumina phase is resolved as white while metastable γ-alumina appears as grey in contrast. Therefore BSE is a powerful technique to analyse the phase distribution in this type of coatings. In order to investigate the solubility distribution achieved by TiO_2 in Al_2O_3 in these microstructures, BSE images of the Al_2O_3-TiO_2 coating were also recorded (Figure 3).

Figure 3.

The BSE images showed a uniform brightness on melted grains while a low intensity of backscattered electrons was detected from softer material. The homogeneity in brightness received from fully melted grains indicates a greater compositional homogeneity compared with that obtained by other works [49] using conventional APS which produces splats with heterogeneous phase compositional distribution. Thus, TiO_2 has been well trapped as solute in the alumina as indicated by BSE micrographs and XRD patterns.

However, only small zones of melted grains show higher brightness, indicating a differentiated phase or different element concentration. Therefore, EDX map revealed that several of the BSE brightest zones correspond to higher concentrations of Ti or Al while others were probably due to the presence of different crystalline phases. Further investigations by backscattered X-ray diffraction could help us to clarify the phase distribution that was previously identified by DRX analysis.

3.3. Nanomechanical properties

Indentations were performed on polished cross-sections in order to acquire the indentation hardness (*H*) and elastic modulus (*E*). Attempts to perform this study on the

coating surface were unsuccessful due to an excessive surface roughness for nanoindentation requirements.

Results show that *H* and *E* profiles tend to decrease after 300 nm in-depth approximately, as figure 4 shows. The decrease of *H* and *E* in-depth was due to the brittle behaviour of the coating as well as by the softer character of unmelted or partially melted material [50].

Figure 4.

The registered load-depth curves (Figure 5) revealed pop-in events when tests overload the 300 nm depth. The failure mechanism was studied by observation of the generated imprints. The Figure 6figure 6 reveals cracks emerging from the edges of each generated imprint. This behaviour indicates a low toughness and justifies the loss of mechanical response observed when load increases.

Figure 5.

Figure 6.

The arithmetic average of *E* and *H* values were calculated between 125 and 300 nm depth ranges. This compromised solution was adopted to avoid the roughness and tip roundness effects at low penetration depths while the crack growth is avoided. The averaged results are screened in Figure 7. The achieved *H* and *E* values are in agreement with previously reported values for similar compositions and projection processes [51,52].

Figure 7.

4. Discussion

These results show that the addition of TiO_2 leads to higher *H* and *E* values. The higher mechanical response when nano-TiO_2 is added to nano-Al_2O_3 suspension in SPS Al_2O_3-13 wt% TiO_2 coatings, as obtained in this work, could be explained by the higher volume of melted material achieved and due to the presence of the hard Al_2TiO_5 spinel formed. Thus, TiO_2 contributes to reduce the amount of partially melted areas and consequently to enhance the mechanical properties of the final coatings.

Although the mechanical properties of SPS Al_2O_3 layers should be improved by diminishing the unmelted volume fraction, it should be pointed out that the spraying parameters used in this study have been optimised, revealing that the window of SPS parameters which allows depositing a continuous, homogeneous and well-bonded coating is more reduced than in conventional powder plasma spraying. As a consequence even the optimal experimental conditions lead to the presence of partially melted material as illustrated in figure 2. Thus, the results obtained in this work are of especial interest as they demonstrate that the addition of TiO_2 is an effective method to reduce the unmelted phases in SPS alumina layers, resulting in a coating with higher mechanical properties.

Conclusions

Al_2O_3 and Al_2O_3-13wt% TiO_2 coatings have been successfully deposited by suspension plasma praying using commercial nanosuspensions as feedstock. Resulting coating's microstructure was fully characterised showing differences in the coating architecture when titanium oxide was added to the suspension feed. Indeed, the results demonstrated that the addition of nano-TiO_2 effectively increases the powder melting leading to

denser coating and to the formation of new hard phases such as aluminium titanate and rutile. However, the proportion of corundum is lower in the Al_2O_3-13wt% TiO_2 layer. Moreover, TiO_2 has been well trapped as solute in the alumina as indicated by BSE micrographs and X-Ray diffraction patterns. Nanoindentation technique confirmed that the addition of TiO_2 leads to both higher hardness and elastic modulus values attributed to the major ratio of melted material achieved.

Acknowledgements

This work has been supported by the Spanish Ministry of Economy and Competitiveness (INNOBAR Project, reference: MAT2012-38364-C03) and it has been co-funded by ERDF (European Regional Development Funds).

References

[1] H. Gleiter, Nanostructured materials: basic concepts and microstructure, Acta Mater. 48 (1) (2000) 1–29.

[2] E. Roduner, Size matters: why nanomaterials are different, Chem. Soc. Rev. 35 (7) (2006) 583–592.

[3] R.W. Siegel, Nanostructured materials: mind over matter, Nanostruct. Mater. 3 (1–6) (1993) 1–18.

[4] M.G. Kanatzidis, Nanostructured thermoelectrics: the new paradigm?, Chem. Mater. 22 (3) (2010) 648–659.

[5] L. Li, T. Zhai, Y. Bando, D. Golberg, Recent progress of one-dimensional ZnO nanostructured solar cells, Nano Energy 1 (1) (2012) 91–106.

[6] K. Jia, T.E. Fischer, Abrasion resistance of nanostructured and conventional cemented carbides, Wear 200 (1–2) (1996) 206–214.

[7] S.C. Tjong, H. Chen, Nanocrystalline materials and coatings, Mater. Sci. Eng. R Rep. 45 (1–2) (2004) 1–88.

[8] M. Gell, Application opportunities for nanostructured materials and coatings, Mater. Sci. Eng. A 204 (1–2) (1995) 246–251.

[9] N.B. Dahotre, S. Nayak, Nanocoatings for engine application, Surf. Coat. Technol. 194 (1) (2005) 58–67.

[10] J.R. Davis, Handbook of thermal spray technology, ASM International, Materials park, 2004.

[11] A.K. Keshri, A. Agarwal, Plasma processing of nanomaterials for functional applications–A review, Nanosci. Nanotechnol. Lett. 4 (2012) 228–250.

[12] P. Fauchais, G. Montavon, R.S. Lima, B.R. Marple, Engineering a new class of thermal spray nano–based microstructures from agglomerated nanostructured particles, suspensions and solutions: An invited review, J. Phys. D: App. Phys. 44 (9) (2011) 93001.

[13] B.R. Marple, R.S. Lima, Engineering nanostructured thermal spray coatings: Process–property–performance relationships of ceramic based materials, Adv. App. Ceram. 106 (5) (2007) 265–275.

[14] E. Sánchez, A. Moreno, M. Vicent, M.D. Salvador, V. Bonache, E. Klyatskina, I. Santacruz, R. Moreno, Preparation and spray drying of Al_2O_3–TiO_2 nanoparticle suspensions to obtain nanostructured coatings by APS, Surf. Coat. Technol. 205 (4) (2010) 987–992.

[15] E.H. Jordan, M. Gell, Y.H. Sohn, D. Goberman, L. Shaw, S. Jiang, M. Wang, T.D. Xiao, Y. Wang, P. Strutt, Development and implementation of plasma sprayed nanostructured ceramic coatings, Surf. Coat. Technol. 146–147 (2001) 48–54.

[16] P.P. Bandyopadhyay, D. Chicot, B. Venkateshwarlu, V. Racherla, X. Decoopman, J. Lesage, Mechanical properties of conventional and nanostructured plasma sprayed alumina coatings, Mech. Mater. 53 (2012) 61–71.

[17] D. Zois, A. Lekatou, M. Vardavoulias, A. Vazdirvanidis, Nanostructured alumina coatings manufactured by air plasma spraying: Correlation of properties with the raw powder microstructure, J. Alloys Compd. 495 (2) (2010) 611–616.

[18] N. Berger-Keller, G. Bertrand, C. Filiare, C. Meunier and C. Coddet, Microstructure of Plasma-Sprayed Titania Coatings Deposited from Spray-Dried Powder, Surf. Coat. Technol.168 (2–3) (2003) 281–290.

[19] F.L. Toma, G. Bertrand, D. Klein, C. Meunier, S. Begin, Development of photocatalytic active TiO_2 surfaces by thermal spraying of nanopowders, J. Nanomater. 2008 (1) (2008) 384171.

[20] D. Wang, Z. Tian, L. Shen, Z. Liu, Y. Huang, Influences of laser remelting on microstructure of nanostructured Al_2O_3–13 wt.% TiO_2 coatings fabricated by plasma spraying, Appl. Surf. Sci. 255 (8) (2009) 4606–4610.

[21] B. Liang, G. Zhang, H.L. Liao, C. Coddet, C.X. Ding, Structure and tribological performance of nanostructured ZrO_2–3 mol% Y_2O_3 coatings deposited by air plasma spraying, J. Therm. Spray Technol. 19 (6) (2010) 1163–1170.

[22] R.S. Lima, B.R. Marple, Nanostructured YSZ thermal barrier coatings engineered to counteract sintering effects, J. Mater. Sci. Technol. A 485 (1–2) (2008) 182–193.

[23] X. Wang, Y. Zhu, L. Du, W. Zhang, The study on porosity and thermophysical properties of nanostructured $La_2Zr_2O_7$ coatings, Appl. Surf. Sci. 257 (21) (2011) 8945–8949.

[24] L. Pawlowski, Suspension and solution thermal spray coatings, Surf. Coat. Technol. 203 (19) (2009) 2807–2829.

[25] R. Vassen, H. Kassner, G. Mauer, D. Stöver, Suspension plasma spraying: Process characteristics and applications, J. Therm. Spray Technol. 19 (1–2) (2010) 219–225.

[26] M. Vicent, E. Sánchez, T. Molina, M.I. Nieto, R. Moreno, Comparison of freeze drying and spray drying to obtain porous nanostructured granules from nanosized suspensions, J. Eur. Ceram. Soc. 32 (5) (2012) 1019–1028.

[27] M. Vicent, E. Sánchez, A. Moreno, R. Moreno, Preparation of high solids content nano–titania suspensions to obtain spray–dried nanostructured powders for atmospheric plasma spraying, J. Eur. Ceram. Soc. 32 (1) (2012) 185–194.

[28] M. Marr, O.Kesler, Permeability and microstructure of suspension plasma-sprayed YSZ electrolytes for SOFCs on various substrates, J. Therm. Spray Technol. 21 (6) (2012) 1334–1346.

[29] Macwan, D.L. Chen, M. Marr, O. Kesler, Residual stresses in suspension plasma sprayed electrolytes in metal-supported SOFC half cells, J. Power Sour. 221 (1) (2013) 397–405.

[30] Guignard, G. Mauer, R. Vassen, D. Stöver, Deposition and characteristics of submicrometer–structured thermal barrier coatings by suspension plasma spraying, J. Therm. Spray Technol. 21 (3–4) (2012) 416–424.

[31] L. Latka, A. Cattini, L. Pawlowski, S. Valette, B. Pateyron, J.P. Lecompte, R. Kumar, A. Denoirjean, Thermal diffusivity and conductivity of yttria stabilized zirconia coatings obtained by suspension plasma spraying, Surf. Coat. Technol. 208 (2012) 87–91.

[32] G. Mauer, A. Guignard, R. Vassen, Plasma spraying of efficient photoactive TiO_2 coatings, Surf. Coat. Technol. 220 (2013) 40–43.

[33] S. Kozerski, F.L. Toma, L. Pawlowski, B. Leupolt, L. Latka, L.M. Berger, Suspension plasma sprayed TiO_2 coatings using different injectors and their photocatalytic properties, Surf. Coat. Technol. 205 (4) (2010) 980–986.

[34] J. Oberste Berghaus, B. Marple, C. Moreau, Suspension plasma spraying of nanostructured WC–12Co coatings, J. Therm. Spray Technol. 15 (4) (2006) 676–681.

[35] R. Tomaszek, L. Pawlowski, L. Gengembre, J. Laureyns, A. Le Maguer, Microstructure of suspension plasma sprayed multilayer coatings of hydroxyapatite and titanium oxide, Surf. Coat. Technol. 201 (16–17) (2007) 7432–7440.

[36] R.B. Heimann, Plasma–spray coating, second ed., Wiley–VCH, 2008.

[37] Rico, P. Poza, J. Rodríguez, High temperature tribological behavior of nanostructured and conventional plasma sprayed alumina–titania coatings, Vac. 88 (1) (2013) 149–154.

[38] R. Yilmaz, A.O. Kurt, A. Demir, Z. Tatli, Effects of TiO_2 on the mechanical properties of the Al_2O_3–TiO_2 plasma sprayed coating, J. Eur. Ceram. Soc. 27 (2–3) (2007) 1319–1323.

[39] M. Harju, M. Järn, P. Dahlsten, J.B. Rosenholm, T. Mäntyl, Influence of long-term aqueous exposure on surface properties of plasma sprayed oxides Al_2O_3, TiO_2 and their mixture Al_2O_3–$13TiO_2$, Appl. Surf. Sci. 254 (22) (2008) 7272–7279.

[40] R. Tomaszek, L. Pawlowski, J. Zdanowski, J. Grimblot, J. Laureyns, Microstructural transformations of TiO_2, Al_2O_3+$13TiO_2$ and Al_2O_3+$40TiO_2$ at plasma spraying and laser engraving, Surf. Coat. Technol. 185 (2–3) (2004) 137–149.

[41] S. Guessasma, M. Bounazef, P. Nardin, T. Sahraoui, Wear behavior of alumina-titania coatings: Analysis of process and parameters, Ceram. Int. 32 (1) (2006) 13–19.

[42] S. Islak, S. Buytoz, E. Ersöz, N. Orhan, J. Stokes, J.M. Saleem Hashmi, M.I. Somunkiran, N. Tosun, Effect on microstructure of TiO_2 rate in Al_2O_3–TiO_2 composite coating produced using plasma spray method, Optoelectron. Adv. Mat. 6 (9–10) (2012) 844–849.

[43] X. Lin, Y. Zeng, X. Zhou, C. Ding, Microstructure of alumina–3wt.% titania coatings by plasma spraying with nanostructured powders, Mater. Sci. Eng. A 357 (1–2) (2003) 228–234.

[44] E.H. Jordan, M. Gell, Y.H. Sohn, D. Goberman, L. Shaw, S. Jiang, M. Wang, T.D. Xiao, Y. Wang, P. Strutt, Fabrication and evaluation of plasma sprayed nanostructured alumina–titania coatings with superior properties, Mater. Sci. Eng. A 301 (1) (2001) 80–89.

[45] G. Darut, E. Klyatskina, S. Valette, P. Carles, A. Denoirjean, G. Montavon, H. Ageorges, F. Segovia, M.D. Salvador, Architecture and phases composition of suspension plasma sprayed alumina–titania sub–micrometer–sized coatings, Mater. Lett. 67 (1) (2012) 241–244.

[46] M. Vicent, E. Sánchez, G. Mallol, R. Moreno, Study of colloidal behaviour and rheology of Al_2O_3–TiO_2 nanosuspensions to obtain free–flowing spray–dried granules for atmospheric plasma spraying, Ceram. Int. 39 (7) (2013) 8103–8111.

[47] R. McPherson, On the formation of thermally sprayed alumina coatings, J. Mater. Sci. 15 (12) (1980) 3141–3149.

[48] Y. Zeng, S.W. Lee, C.X. Ding, Plasma spray coatings in different nanosize alumina, Mater. Lett. 57 (2002) 495–501.

[49] R. Venkataraman, S.P. Singh, B. Venkataraman, D.K. Das, L.C. Pathak, S. Ghosh Chowdhury, R.N. Ghosh, D. Ravichandra, G.V.N. Rao, K. Nair, R. Kathirkar, A scanning electron microscopic study to observe the changes in the growth morphology of the α phased Alumina–13 wt.% titania coatings during plasma spraying, Surf. Coat. Technol. 202 (21) (2008) 5074–5083.

[50] E. Rayón, V. Bonache, M.D. Salvador, J.J. Roa, E. Sánchez, Hardness and Young's modulus distributions in atmospheric plasma sprayed WC–Co coatings using nanoindentation, Surf. Coat. Tech. 205 (17–18) (2011) 4192–4197.

[51] J. Rodriguez, A. Rico, E. Otero, W.M. Rainforth, Indentation properties of plasma sprayed Al_2O_3–13% TiO_2 nanocoatings, Acta Mater. 57 (11) (2009) 3148–3156.

[52] E. Bannier, G. Darut, E. Sánchez, A. Denoirjean, M.C. Bordes, M.D. Salvador, E. Rayón, H. Ageorges, Microstructure and photocatalytic activity of suspension plasma sprayed TiO_2 coatings on steel and glass substrates, Surf. Coat. Technol. 206 (2–3) (2011) 378–386.

Tables

Table 1. Main characteristics of the commercial suspensions as provided by the supplier (Evonik Degussa GmbH, Germany).

Table 2. Main SPS spraying parameters.

Figure captions

Figure 1. X-Ray diffraction pattern of suspension plasma sprayed Al_2O_3 (down) and Al_2O_3-13wt%TiO_2 (up) coatings.

Figure 2. Secondary electron FEG-SEM cross-sectional micrographs of a) Al_2O_3-13wt%TiO_2 and b) Al_2O_3 SPS coatings.

Figure 3. BSE and EDX maps of the Al_2O_3-13wt%TiO_2 coating.

Figure 4. Hardness and elastic modulus profiles acquired by nanointendation for Al_2O_3 and Al_2O_3-13 wt% TiO_2 coatings.

Figure 5. Load versus penetration depth curves acquired by nanoindentation at the experimented coatings.

Figure 6. Optical microscope image showing cracks emerging from the edges of the residual Berkovich imprint

Figure 7. Hardness and Young moduli results of Al_2O_3 and Al_2O_3 – 13 wt% TiO_2 coatings acquired by nanoindentation

Figure-1

Click here to download high resolution image

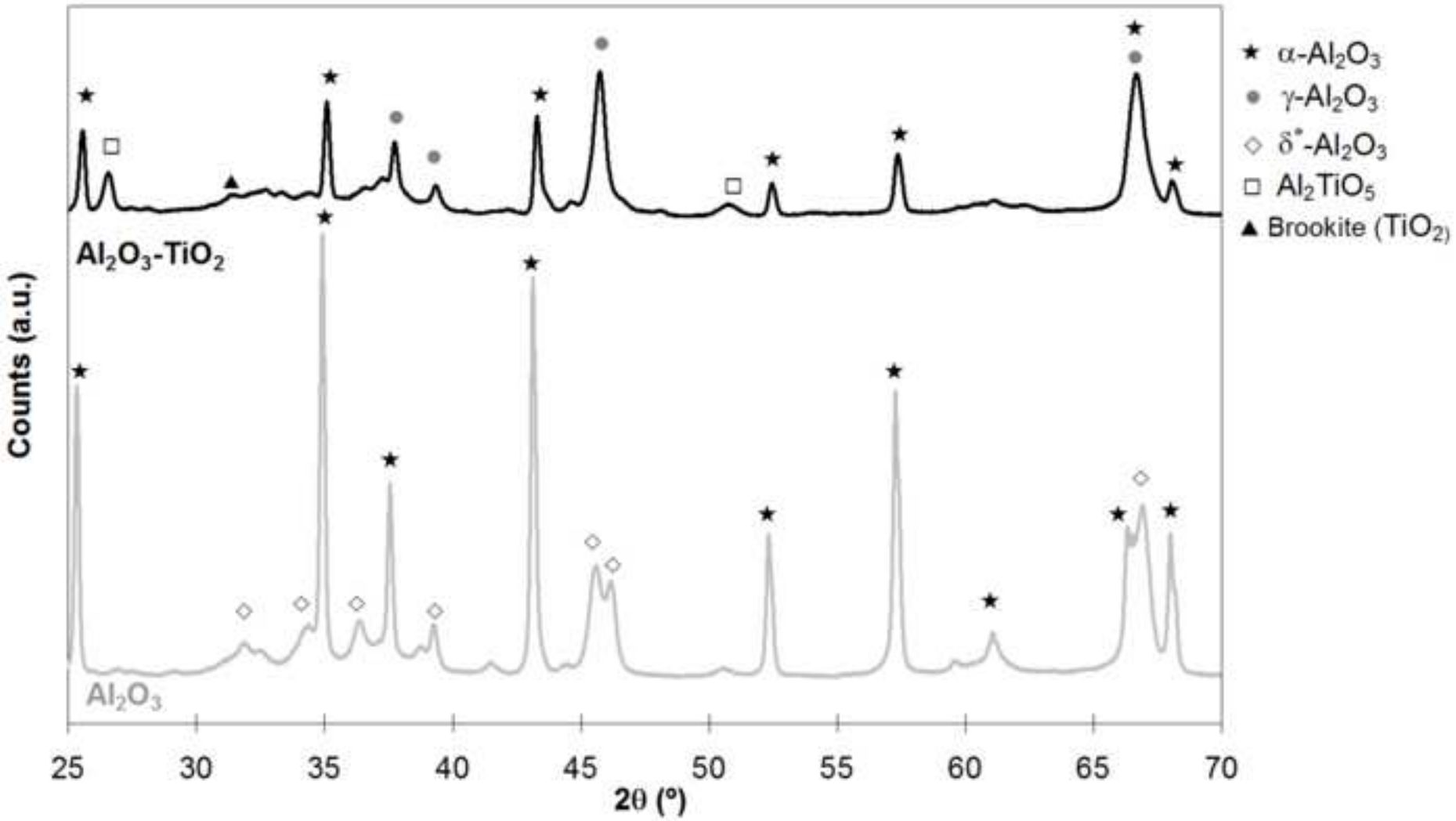

Figure-2

Click here to download high resolution image

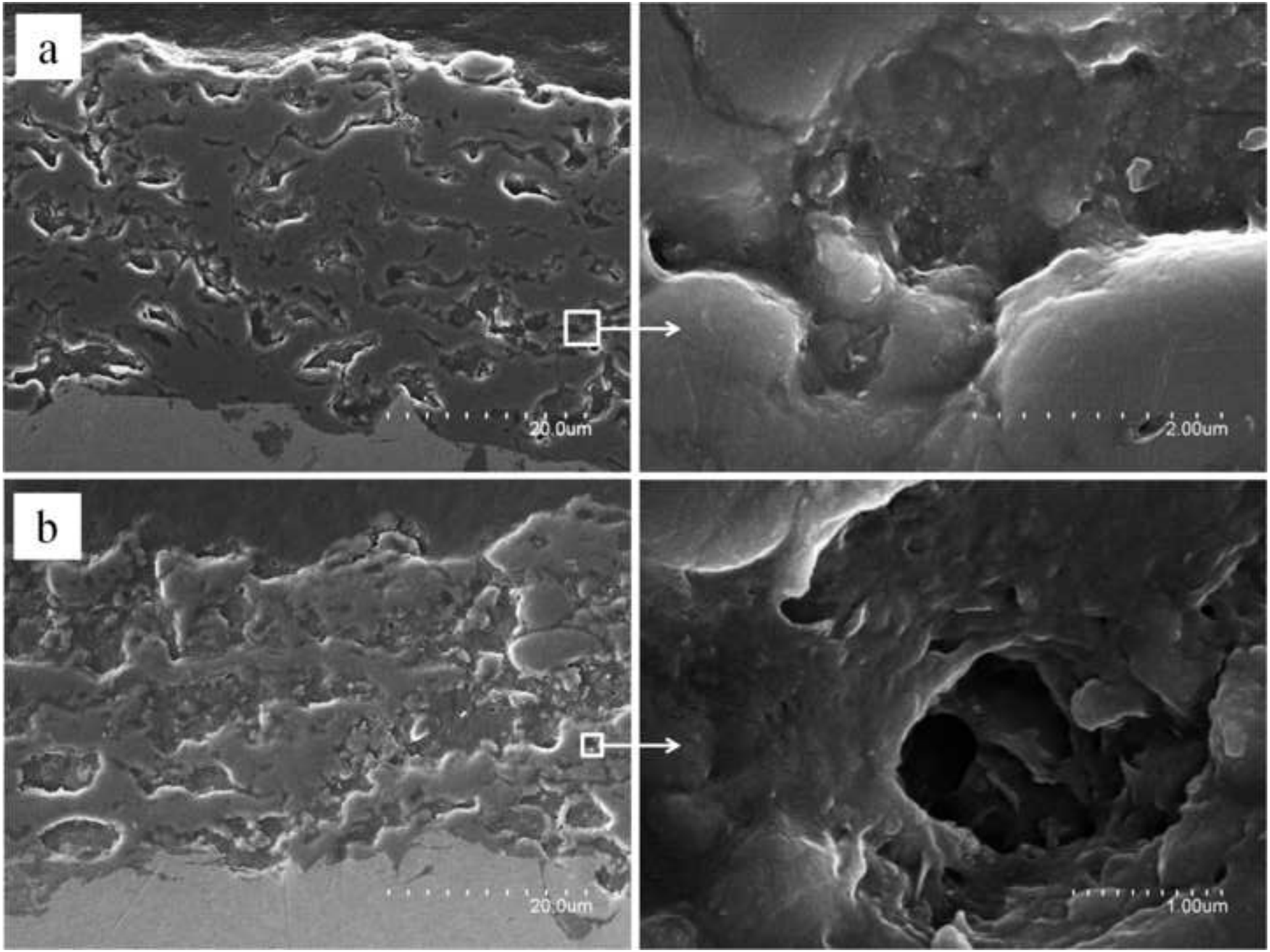

Figure-3

Click here to download high resolution image

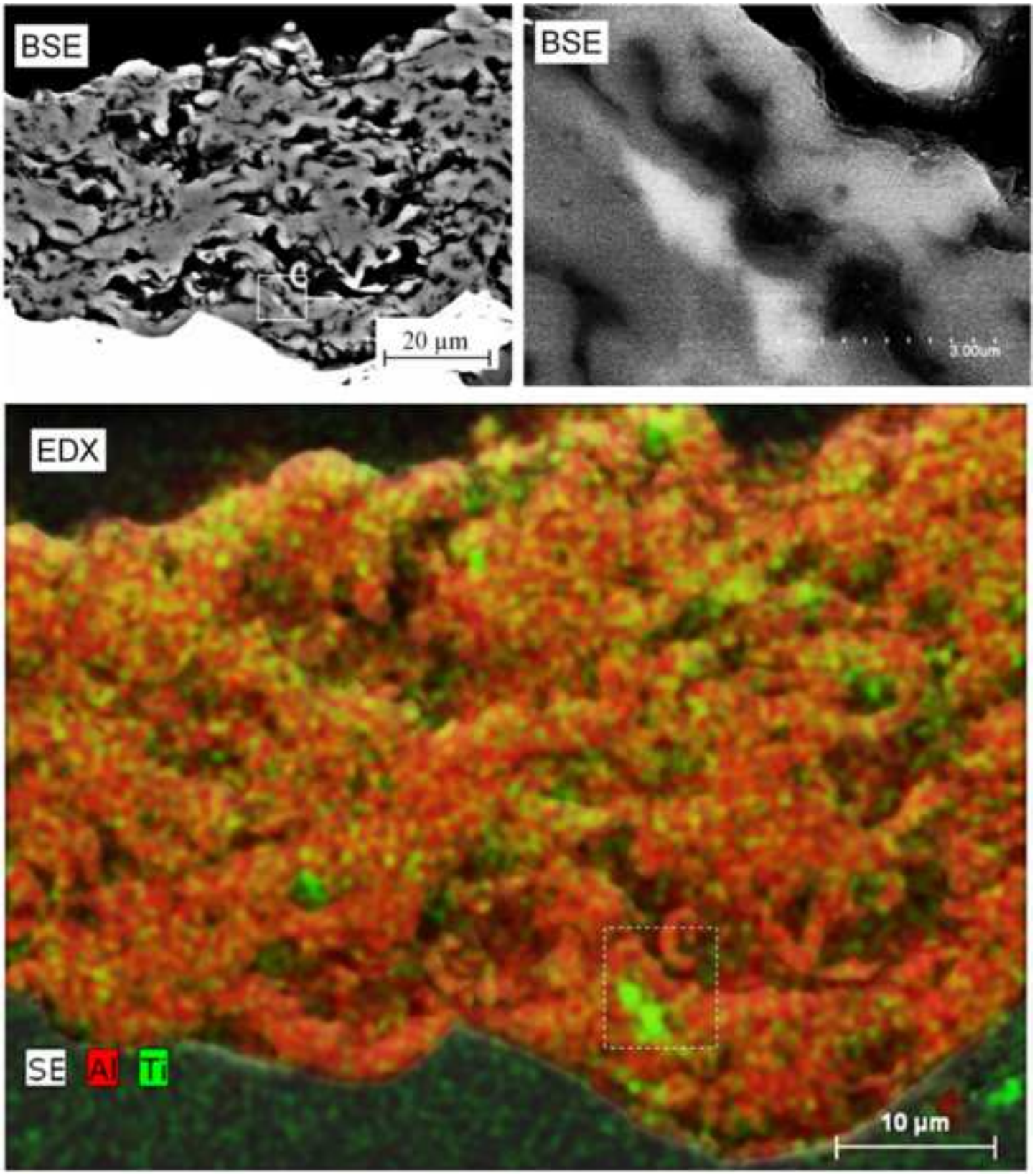

Figure-4

Click here to download high resolution image

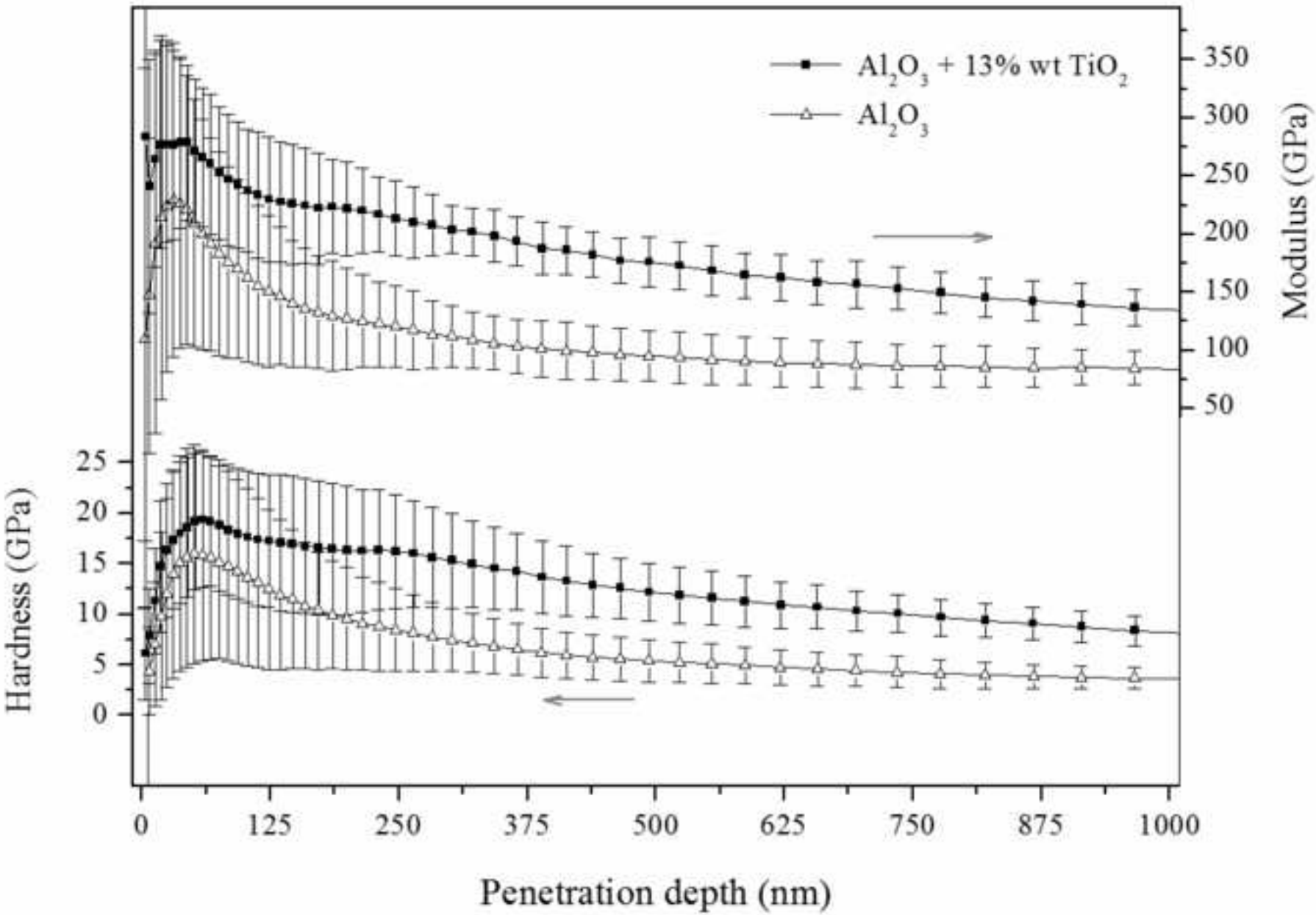

Figure-5

Click here to download high resolution image

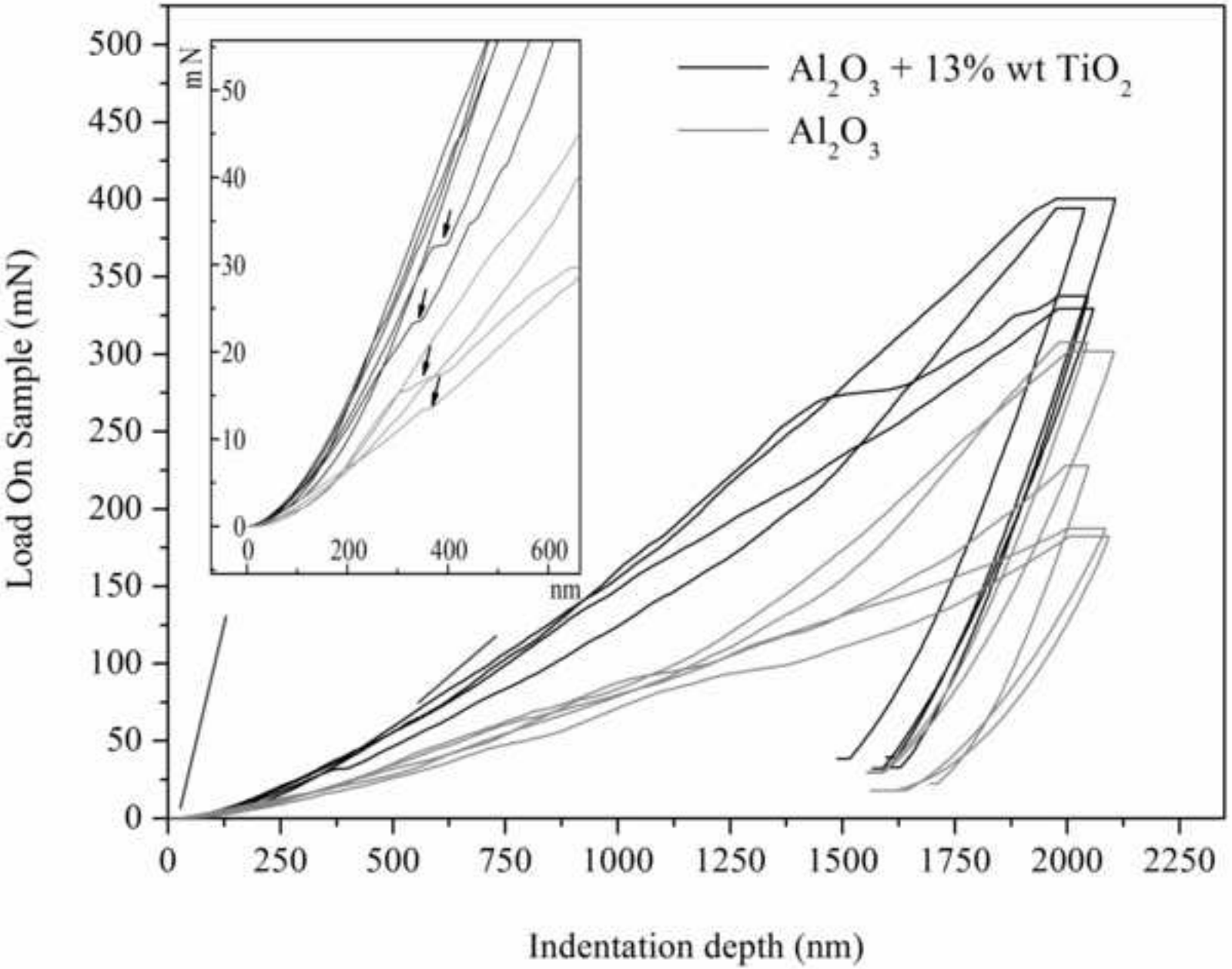

Figure-6

Click here to download high resolution image

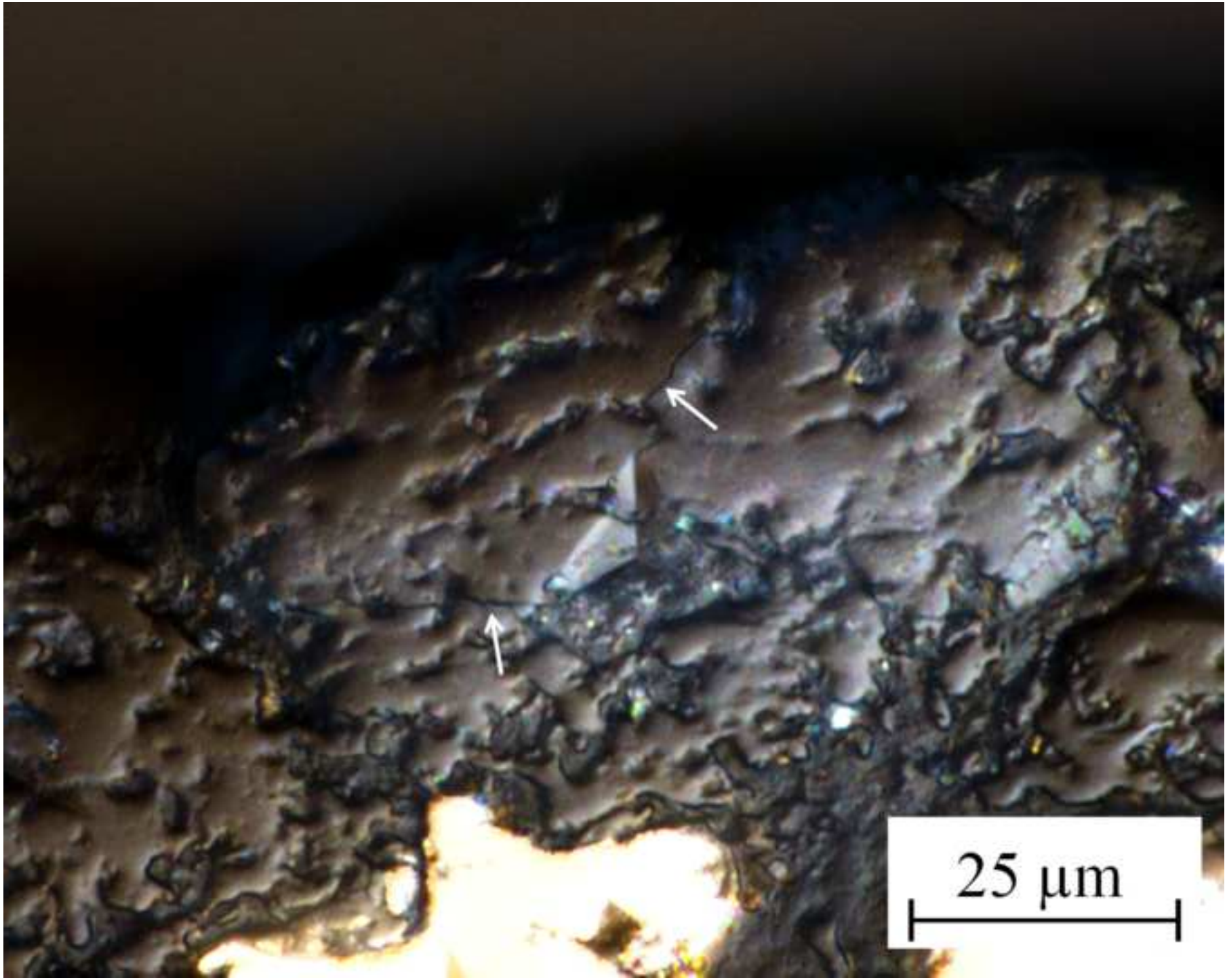

Figure-7

Click here to download high resolution image

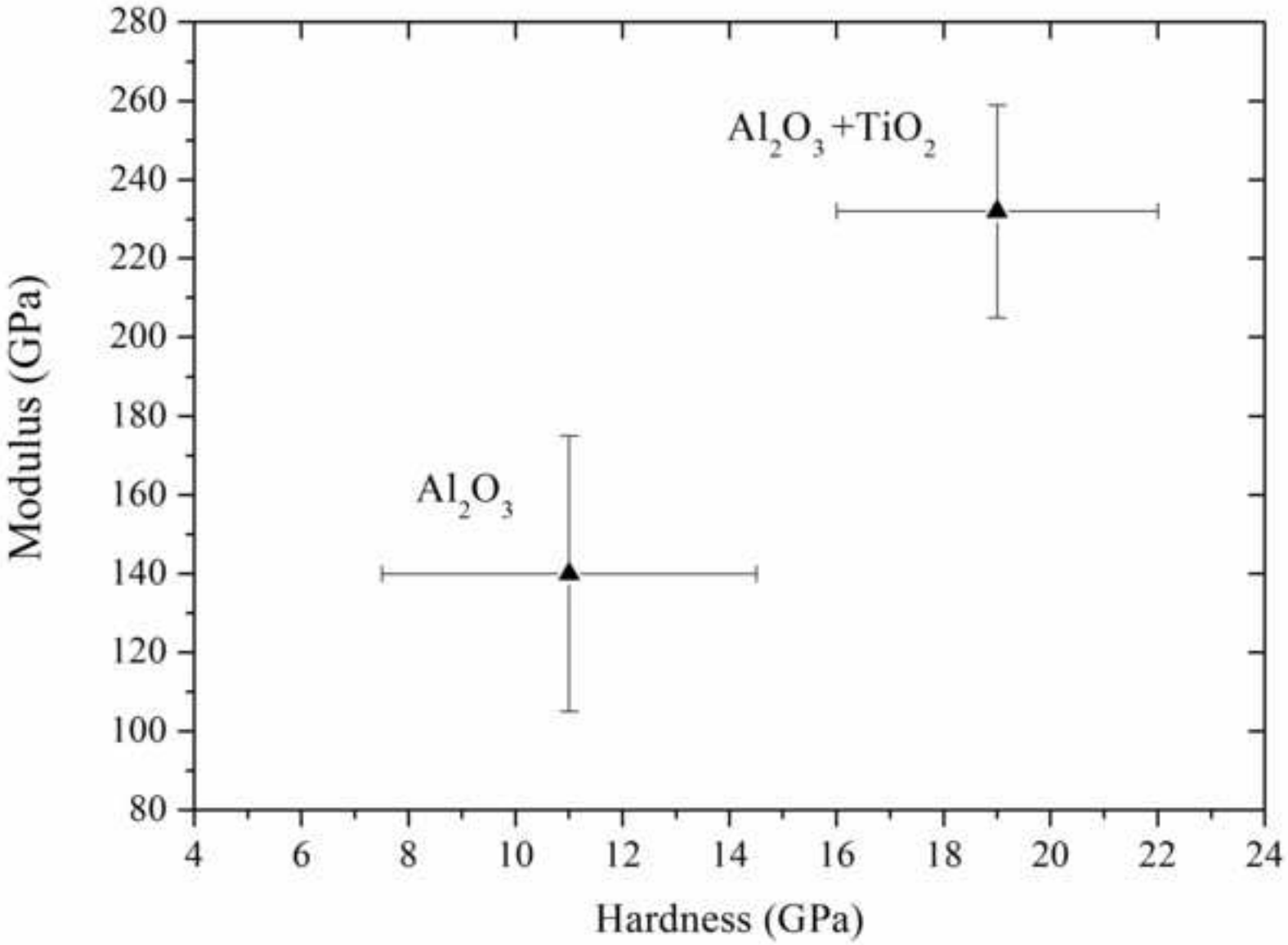

Table-1

Reference	Suspension type	Solids content (wt%)	pH	Viscosity (mPa·s)	Mean aggregate size (nm)	Density at 20 °C (g/cm^3)
AERODISP VP630X	Al_2O_3	30.0 ± 0.1	3.0-5.0	≤ 2000	140	1.27
AERODISP W740X	TiO_2	40.0 ± 0.1	5.0-7.0	≤ 1000	≤ 100	1.41

Table 1. Main characteristics of the commercial suspensions as provided by the supplier (Evonik Degussa GmbH, Germany).

Table-2

Ar (l/min)	H_2 (l/min)	Arc intensity (A)	Spraying distance (mm)	Spraying velocity (m/s)	Suspension feed rate (ml/min)	Injector diameter (μm)
37	8	700	30	1	27	150

Table 1. Main SPS spraying parameters.